Evaluation of B-52 Structural Response to Random Turbulence with Stability Augmentation Systems

JOHN B. DEMPSTER* AND KENNETH L. ROGER†
The Boeing Company, Wichita, Kansas

A theoretical evaluation of the structural performance of benefits to be expected after installing a state-of-the-art stability augmentation system (SAS) on the B-52 is presented. The new system is expected to provide additional stability in the airplane rigid body motions and the low-frequency structural vibration modes. The mathematical model used in this study included rigid body motions, a large number of normal vibration modes, control surface rotations, and the SAS transfer functions. The dynamic response of the airplane to random atmospheric turbulence was determined using harmonic analysis techniques with provisions made to include the effects of nonlinearities due to SAS saturation. Quantitative estimates of the changes in airplane structural response indicate that fatigue-damage accumulation rates and peak-load amplitudes, due to atmospheric turbulence, can be significantly reduced without degrading the flutter margin.

Nomenclature

A	=	ratio of rms response to rms gust velocity
$A_{\dot{}} \times_{\dot{}} N_0$	=	$(0.5/\pi) \times$ ratio of rms response rate to rms gust velocity
$C_1, \ldots, C_9$	=	coefficient matrices in airplane equations of motion
D	=	damage accumulation rate, from Miner's linearized fatigue-failure theory
K	=	Wagner's lift-growth function
L	=	scale of turbulence (1000 ft)
$M(y)$	=	average number of y-level crossings with positive slope for a specified response, per second
N_i	=	average number of cycles required for fatigue failure at the ith incremental stress level
N_0	=	average number of mean-level crossings with positive slope for a specified response, per second
P_1, P_2	=	turbulence parameters used in functional representation of $f(\sigma_u)$
V	=	airplane true airspeed
b_1, b_2	=	turbulence parameters used in functional representation of $f(\sigma_u)$
$f(\sigma_u)$	=	probability density distribution of rms gust velocity
η_i	=	number of cycles of applied stress per second at the ith incremental stress level
q	=	displacement vector in equations of motion
y	=	response level
$\phi(\omega)$	=	power spectral density function
ψ	=	Küssner's lift-growth function
α_g	=	$(1/V) \times$ vertical gust velocity at airload panel
β_g	=	$(1/V) \times$ lateral gust velocity at airload panel
σ_u	=	rms gust velocity
ω	=	frequency, rad/sec

Introduction

AN Air Force sponsored study was conducted by The Boeing Company during 1964 and 1965 to determine the changes to the B-52 flight control and SAS which would provide meaningful improvements in the airplane structural life and the aerodynamic and structural stability in severe turbulence. The results of the study program indicated that significant reductions in structural fatigue and peak loads could be expected if a state-of-the-art SAS were installed on the B-52. Development of an improved SAS was continued, based on the results of this initial study. This paper presents a description of the structural analyses conducted and a summary of the results obtained during further definition of the SAS.

The present B-52G/H control system provides longitudinal control through a tab driven, full span, 10% chord elevator. The stabilizer is an all movable surface providing longitudinal trim. Directional control is provided by a tab driven, full span, 10% chord rudder. Seven hydraulically actuated spoilers are mounted on the upper surface of each wing. Lateral control of the airplane is provided by independent extension of the spoilers on either wing. The spoilers are also used as airbrakes.

The present airplane configuration includes an electromechanical yaw damper (EYD). This system senses yaw rate of the airplane with a rate gyro to command a servo motor position which, in turn, positions a bobweight and the rudder stability tab. The rate-gyro signal is shaped by an electrical network to sharply attenuate EYD response at the structural mode frequencies. When the EYD is turned off, a magnetic yaw damper continues to provide Dutch-roll damping. Lateral acceleration is sensed for the magnetic yaw damper by a bobweight mounted in the vertical tail. The bobweight motion is damped by a magnetic field, providing the phasing required for Dutch-roll damping. The bobweight has a mechanical linkage to the rudder stability tab. The B-52 also has a conventional autopilot system that provides attitude stabilization but does not significantly change the short period pitch response.

In the following sections, the general analytical approach is described, including ground rules, SAS variations considered, and the SAS selected for developmental testing. Brief discussions of the B-52 mathematical model considered are presented, including descriptions of the structural model, aerodynamic considerations, equations of motion, and method of solution. The random analysis methods used are described, including the calculation of transfer functions and response parameters, and the use of these parameters along with the atmospheric turbulence model to obtain response statistics. Finally, a summary is presented of the significant analysis results obtained. These results are presented in terms of the expected SAS effect on fatigue damage, peak load, elastic and rigid body stability, and crew-compartment acceleration. Throughout the paper, primary emphasis

Presented as Paper 66-998 at the AIAA Third Annual Meeting, Boston, Mass., November 29–December 2, 1966; submitted December 9, 1966; revision received June 26, 1967. [6.01,7.05,7.10]

* Group Engineer, Loads Group, Wichita Division. Associate Fellow AIAA.

† Structures Engineer, Loads Groups, Wichita Division. Member AIAA.

is given to the structural analyses and the evaluation of the SAS based on the B-52 structural performance.

Analytical Approach

A general description of the analytical approach is given in the following paragraphs. These details are presented in order to provide some insight into the factors affecting the selection of a state-of-the-art SAS configuration.

Ground Rules

The significant decisions made early in the program are presented and discussed below. These ground rules influenced the improved SAS design and are considered an important part of the description of the analytical approach:

1) The program will include yaw axis and pitch axis SAS.

2) The yaw and pitch SAS will use existing rudder and elevator surfaces. The maximum force output of the rudder and elevator actuators will provide control surface travel, consistent with the limit strength of the associated structure.

3) The surface actuation will be accomplished using high-performance hydraulic actuators. This system was selected and the actuators were located in the fin and stabilizer to provide positive actuation of the control surfaces with suitable frequency response characteristics.

SAS Selected for Development

A variety of inputs to the rudder and elevator feedback loops were studied. Lateral-directional inputs included yaw rate, side acceleration, and combinations of these. Pitch-axis inputs included pitch rate and vertical acceleration. Several structural locations for the motion sensors were also considered. Changes in SAS feedback loop gains for changing flight conditions were considered desirable and studies were made to establish suitable gain variations with altitude, impact pressure, and several other parameters.

The yaw SAS selected for development uses a yaw-rate signal and a side acceleration signal as feedback loop inputs. The signal from the rate gyro is predominant at Dutch-roll frequencies, while the accelerometer signal is predominant at the higher structural mode frequencies. The accelerometer is located in the upper aft fuselage beneath the vertical tail. To reduce the requirement for low-pass filtering of the yaw-rate signal, the yaw-rate gyro is located further forward in the fuselage. The pitch SAS uses a pitch-rate signal only. The pitch-rate gyro is located midway between the wing and the tail.

Both SAS have a variable gain, automatically controlled from a Pitot-static source. The yaw SAS authority is limited to 10 of the 19 deg available for the rudder. The pitch SAS authority is limited to 5 of the 19 deg available for the elevator.

Dynamic Equations of Motion

The airplane dynamic equations of motion were in the following form:

$$[C_1]\{q''\} + [C_2]\{q'\} + [C_3]\{q\} + [C_4]\{K^*q''\} + [C_5]\{K^*q'\} + [C_6]\left\{\frac{\alpha_g}{\beta_g}\right\}_{\text{fuselage}} + [C_7]\left\{\frac{\psi^*\alpha_g'}{\psi^*\beta_g'}\right\}_{\text{wing}} + [C_8]\left\{\frac{0}{\psi^*\beta_g'}\right\}_{\text{vertical tail}} + [C_9]\left\{\frac{\psi^*\alpha_g'}{\psi^*\beta_g'}\right\}_{\text{horizontal tail}} = \{0\} \quad (1)$$

Equation (1) is written in terms of both the symmetric (longitudinal) equations of motion and the antisymmetric (lateral-directional) equations of motion. In general, however, the symmetric and antisymmetric equations of motion are not coupled and are treated separately in subsequent solutions. As explained in a later section, the symmetric and antisymmetric responses are combined prior to the structural performance evaluation.

Structural Model

The airplane inertia and elastic characteristics were idealized, using the lumped parameter method. The distributed mass and stiffness properties of the airplane were represented by 86 discrete mass points connected by weightless springs. The springs and discrete masses were assigned appropriate properties to represent the distributed stiffness and mass properties of the corresponding element of the airplane.

Normal airplane symmetric and antisymmetric vibration modes were computed for the idealized system. The vibration analysis and selection of vibration modes to be included in the equations of motion were accomplished in two steps. Cantilevered vibration modes were computed for the wing, stabilizer, vertical tail, nacelles, forward fuselage, and aft fuselage. A total of 40 cantilevered modes, calculated for the various airplane elements, were then selected for a coupled airplane vibration analysis. These included the first 15 wing modes, four stabilizer modes, four vertical tail modes, three inboard nacelle modes, three outboard nacelle modes, three forward fuselage modes, and eight aft fuselage modes. In each case, the modes selected were the lower-frequency cantilever vibration modes. Symmetric and antisymmetric free-free orthogonal airplane vibration modes were calculated in terms of the selected cantilever modes and appropriate rigid body motions that were introduced to remove the cantilever mode constraints. These coupled airplane vibration modes, along with appropriate rigid body degrees of freedom, were then used in the airplane equations of motion to represent the airplane mass and stiffness properties.

Aerodynamic Considerations

The airloads acting on the airplane were expressed in terms of the aerodynamic lift and moment acting on 60 panels of the wing, stabilizer, vertical tail, and fuselage due to gusts, airplane motions, and control surface rotations. The lift and moment for each airload panel on the wing, stabilizer, and vertical tail were expressed in terms of two-dimensional airfoil theory modified to include the Küssner and Wagner lift-growth functions, the effects of finite span by Weissinger lifting-line theory, and an experimental correction for compressibility. The resulting three-dimensional section lift and moment coefficients included the circulatory aerodynamic coupling between the airload panels. The noncirculatory loads were formulated in a manner to act independently on each airload panel. The fuselage loads were all considered noncirculatory.

Degrees of Freedom

The symmetric or longitudinal dynamic equations of motion were written in terms of rigid body vertical translation and pitch and 28 of the lowest-frequency symmetric airplane coupled vibration modes. To include the pitch SAS, degrees of freedom for the elevator transfer function were added. A maximum of 35 degrees of freedom was used in the symmetric analyses. The antisymmetric or lateral-directional dynamic equations of motion were written in terms of rigid body side translation, roll, and yaw and 27 antisymmetric airplane coupled vibration modes. Except for selection of the airplane mode including vertical tail torsion, these were the lowest-frequency modes. To include the EYD, degrees of freedom for the rudder and the rudder stability tab transfer function were added. To include the yaw SAS, degrees of freedom for the rudder transfer function were added. A maximum of 37 degrees of freedom was used in the antisymmetric analyses.

The symmetric vibration modes ranged in frequency from 0.7 to 32 cps and the antisymmetric vibration modes ranged

in frequency from 1.1 to 20 cps. The use of a large number of flexible vibration modes was necessary to provide proper aeroelastic deflections of the airplane over the frequency range of interest (0 to 10 cps) in gust dynamic response analyses. The fin torsion mode, at 20 cps, was the highest-frequency antisymmetric vibration mode included in the equations of motion, and was found to be a significant contributor to aerodynamic tail loads even at Dutch-roll frequencies. Also, a large number of vibration modes were required to provide structural stability information.

Calculation of Response Parameters

Power spectral density analysis techniques were used to predict the statistical properties of airplane responses due to random atmospheric turbulence. These response statistics were then used to estimate the fatigue-damage rates, the maximum expected load, stability information, and crew-compartment acceleration environment.

The determination of response power spectra depends on a knowledge of the power spectral density of atmospheric turbulence and the frequency response functions of the airplane. The following equation defines a response spectrum for a single-input linear system:

$$\phi_{\text{response}}(\omega) = |T(\omega)|^2 \phi_{\text{turbulence}}(\omega) \tag{2}$$

The theoretical methods used to calculate the airplane frequency response functions are summarized in following paragraphs along with a description of the atmospheric turbulence model considered. Also, the methods used in calculating the response parameters and response statistics are described. This description includes the methods for calculating the total response to vertical and lateral atmospheric turbulence and the methods used to account for the nonlinearities due to SAS operation.

Frequency Response Functions

The theoretical frequency response functions were calculated from the dynamic equations of motion given by Eq. (1). The frequency response equations were obtained by letting the gust input be a unit impulse and taking the Fourier transform of Eq. (1). The response equations were then in terms of a frequency argument for a unit gust velocity and were solved algebraically for complex motion frequency response functions. Load or stress frequency response functions were then computed by summing the resulting airload and inertial load responses. The complex load and motion frequency responses were calculated at a sufficient number of frequencies (usually about 250) to fully define the significant peaks between zero and 10 cps.

Atmospheric Turbulence Model

The atmospheric turbulence model used in the analysis is based on B-52 Vgh data derived in Ref. 1. The statistical description of the atmospheric turbulence environment is defined in terms of spectral density functions and probability density distributions of the rms gust velocities. The total turbulence environment was considered in terms of vertical and lateral gust components. A rolling gust component was used in early studies, but was found to have negligible effect on the structural performance evaluation of the SAS.

The gust power spectral density function used in this study is defined by

$$\phi_{\text{turbulence}}(\omega) = \frac{\sigma_u^2 L}{\pi V} \frac{1 + 3(\omega L/V)^2}{[1 + (\omega L/V)^2]^2} \tag{3}$$

The scale of turbulence (L) considered was 1000 ft. The probability density distribution of rms gust velocity is defined by

$$f(\sigma_u) = \frac{P_1}{b_1}\left(\frac{2}{\pi}\right)^{1/2} \exp\left(-\frac{\sigma_u^2}{2b_1^2}\right) + \frac{P_2}{b_2}\left(\frac{2}{\pi}\right)^{1/2} \exp\left(-\frac{\sigma_u^2}{2b_2^2}\right) \tag{4}$$

The turbulence parameters are given in Table 1.

Table 1 Turbulence parameters

Altitude	P_1	b_1	P_2	b_2
Low level (contour)	0.80	3.6	0.20	4.2
Cruise (30–40,000 ft)	0.13	1.8	0.01	4.8

Response Parameters

The response parameters are related to the response spectrum as follows:

$$A = \frac{1}{\sigma_u}\left[\int_0^\infty \phi_{\text{response}}(\omega)d\omega\right]^{1/2} \tag{5}$$

$$N_0 = \frac{1}{2\pi A \sigma_u}\left[\int_0^\infty \omega^2 \phi_{\text{response}}(\omega)d\omega\right]^{1/2} \tag{6}$$

These response parameters were obtained by numerical integration of the calculated response spectrum over a truncated frequency range of zero to 10 cps.

For a stress response that is sensitive to both vertical and lateral turbulence components, the total stress response spectrum is computed as

$$\phi_{\text{response total}}(\omega) = \phi_{\text{response vertical}}(\omega) + \phi_{\text{response lateral}}(\omega) \tag{7}$$

Equation (7) is dependent on the turbulence model assumption that the vertical and lateral components are statistically independent. This assumption has been verified during Boeing B-52 gust measuring programs. Subsequent total response parameters are obtained by Eqs. (5) and (6).

Response Statistics

The response statistics are defined by the response parameters and the probability density distribution of the rms gust velocities as

$$M(y) = \int_0^\infty N_0 f(\sigma_u) \exp\left(\frac{-y^2}{2A^2\sigma_u^2}\right) d\sigma_u \tag{8}$$

For a linear system, substitution of Eq. (4) into (8) yields

$$M(y) = N_0 P_1 \exp(-y/b_1 A) + N_0 P_2 \exp(-y/b_2 A) \tag{9}$$

Nonlinearities caused by limiting the control surface deflections and SAS operation were accounted for initially by use of the analog computer. Several analog simulation runs were made to define A and N_0 as a function of σ_u, then Eq. (8) was solved numerically to find $M(y)$ vs y. The analog solutions indicated that the response in the nonlinear region was still essentially Gaussian. Also, for small values of σ_u the analog values were in agreement with digital values for the linear SAS analysis and at large values of σ_u, analog A and N_0 values approached the linear system digital values for the airplane with fixed controls. These observations led to a method of predicting nonlinear response parameters based on two linear analyses shown in Figs. 1–4.

The slopes below the breakpoints in Figs. 1 and 2 were determined from analyses of the appropriate systems with no control deflection limits. The slopes above the breakpoint were determined from an analysis of the airplane with controls fixed. The value of σ_u at the breakpoint was estimated by

$$\sigma_{u\text{breakpoint}} = \frac{(0.707) \times (\text{control surface limit})}{A_{\text{control surface rotation}}} \tag{10}$$

The data in Figs. 1 and 2 are replotted in terms of A and N_0 vs σ_u in Figs. 3 and 4. The response statistics for these non-

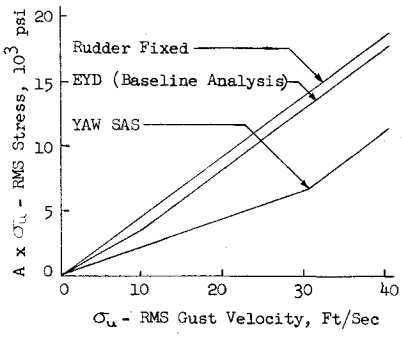

Fig. 1 Fin station 135 spar rms stress vs rms gust velocity.

linear systems were then estimated by considering this variation of A and N_0 with σ_u and numerically integrating Eq. (8).

Evaluation of SAS Structural Performance

The evaluation of SAS structural performance was accomplished by comparing analysis results with SAS to those for the baseline airplane. The baseline airplane was considered to be the airplane with the EYD and no pitch SAS. Results

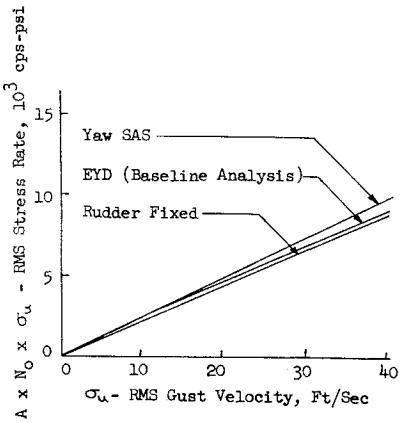

Fig. 2 Fin station 135 spar rms stress rate vs rms gust velocity.

of the structural performance evaluation of the SAS in terms of fatigue damage and peak load are presented in the following paragraphs. Results are also presented showing the effect of SAS on the stability of the low-frequency degrees of freedom and the effect on crew-compartment acceleration.

Fatigue Damage

The general method of analysis used in the calculation of fatigue damage is based on the linear cumulative damage theory as presented by M. A. Miner in Ref. 2. This theory states that damage accumulation in a structural element is equal to the summation of the ratio of the number of cycles

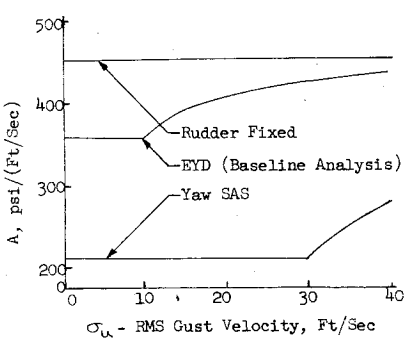

Fig. 3 Fin station 135 spar A vs rms gust velocity.

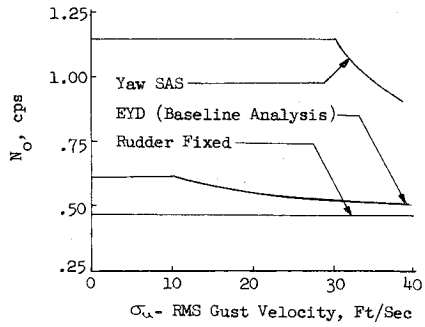

Fig. 4 Fin station 135 spar N_0 vs rms gust velocity.

of applied stress of a given magnitude to the number of cycles to failure at that stress:

$$D = \sum_{i=1}^{m} \frac{\eta_i}{N_i} \tag{11}$$

The cycles to failure curves were derived from B-52 full-scale, component, and specimen cyclic tests. The applied stress history was estimated from Eq. (8) for each structural location of interest. Fatigue-damage rates were then computed for both the baseline airplane and the airplane with SAS.

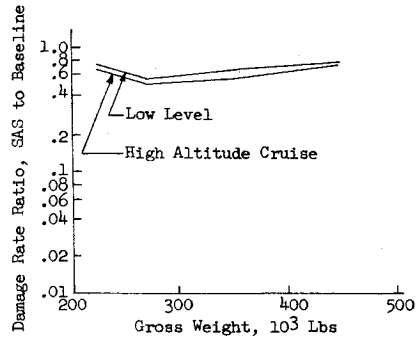

Fig. 5 Ratio of fatigue damage rate due to turbulence, wing station 899 stiffener 3.

The expected decrease in turbulence induced fatigue damage with the SAS is presented in Figs. 5–8 for selected structural locations. The ratio of the fatigue-damage rate for the airplane with the SAS to that of the baseline airplane is plotted vs gross weight for both cruise and low-level operations. Figure 5 presents the expected fatigue-damage decrease for a wing lower surface location. Figures 6–8 present similar information for locations in the aft fuselage, vertical tail, and horizontal tail.

Maximum Expected Load

The maximum expected load due to atmospheric turbulence is that load level expected to occur only once during a given

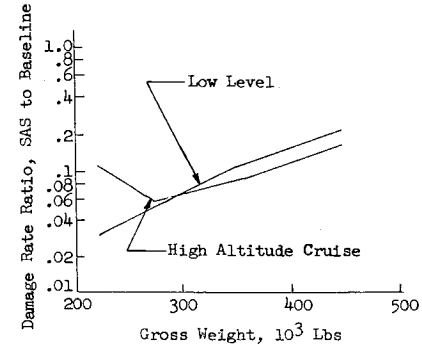

Fig. 6 Ratio of fatigue damage rate due to turbulence, body station 1028 upper longeron.

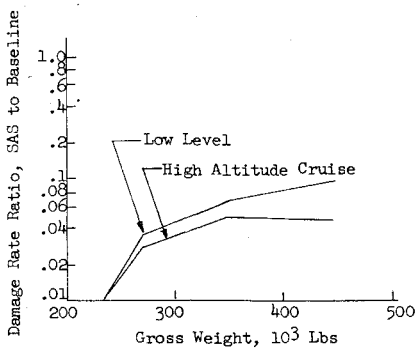

Fig. 7 Ratio of fatigue damage rate due to turbulence, fin station 135 spar.

service period for the airplane. This maximum expected load will vary as a function of the usage of the airplane and the atmospheric turbulence environment. The prediction of peak load using power spectral analysis methods is based on airplane response and turbulence statistics. When it is desired to find the probable maximum load reached during a given number of flight hours, y is computed using Eq. (8) where $M(y) = 0.5/(\text{number of hours})$. The 0.5 factor is

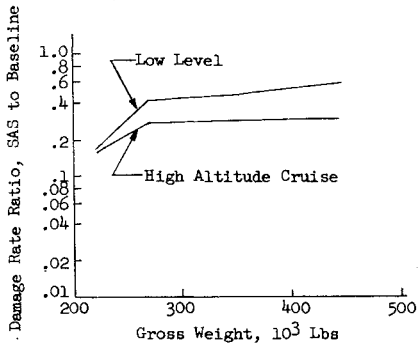

Fig. 8 Ratio of fatigue damage rate due to turbulence, horizontal stabilizer buttock line 32 main spar.

used because either a positive or a negative incremental load greater than y is considered to be a significant crossing. With the steady-state load known, the maximum expected load is the steady-state load plus the predicted peak incremental value. The minimum expected load is the steady-state load minus the predicted peak incremental value.

For the purpose of calculating the effect of the SAS on expected peak load, the usage was arbitrarily taken as 5300 hr high-altitude cruise and 500 hr at low level. Therefore, for a low-level flight condition, the peak load expected during 500 hr was computed for both the baseline airplane and the airplane with the SAS. For a cruise flight condition, the

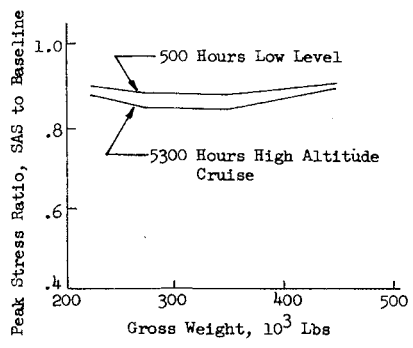

Fig. 9 Ratio of expected peak incremental stress due to turbulence, wing station 899 stiffener 3.

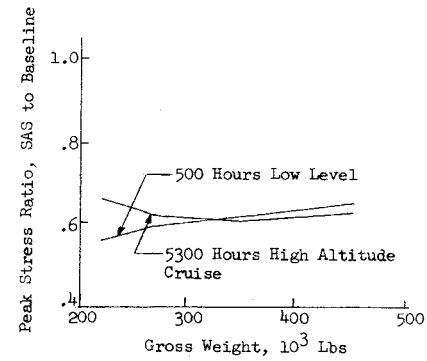

Fig. 10 Ratio of expected peak incremental stress due to turbulence, body station 1028 upper longeron.

corresponding peak loads expected in 5300 hr of flight were computed.

The expected decrease in turbulence induced peak stress with the SAS is presented in Figs. 9–12 for selected structural locations. The ratio of the peak stress for the airplane with the SAS to that of the baseline airplane is plotted vs gross weight for both cruise and low-level operations. Figure 9 presents the expected decrease in peak stress for a wing lower-surface location. Figures 10–12 present similar in-

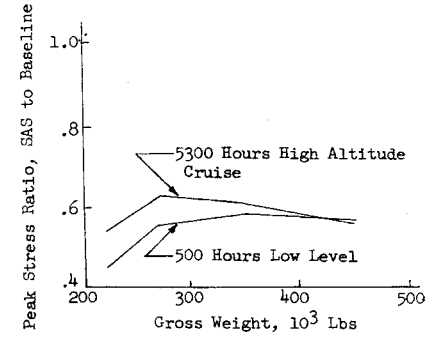

Fig. 11 Ratio of expected peak incremental stress due to turbulence, fin station 135 spar.

formation for structural locations in the aft fuselage, vertical tail, and horizontal tail.

Stability

An objective of the SAS development program was to provide additional aerodynamic and structural stability in severe turbulence. This has been accomplished by increased authority of the SAS and improved frequency response of the SAS.

The yaw SAS rudder authority was selected at 10°, which is a factor of 3 increase in displacement authority over the

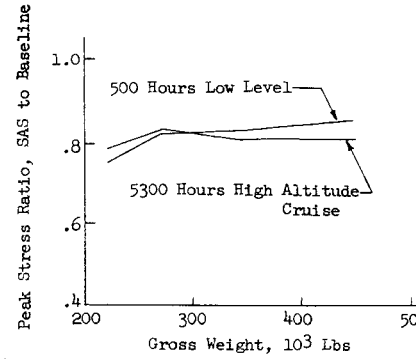

Fig. 12 Ratio of expected peak incremental stress due to turbulence, horizontal stabilizer buttock line 32 main spar.

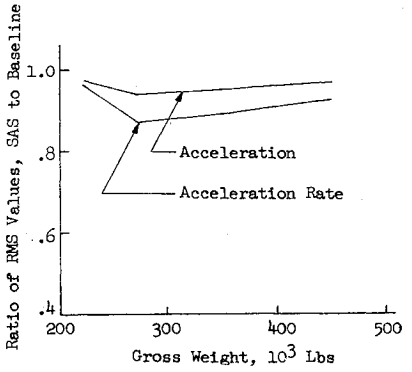

Fig. 13 Ratio of rms vertical acceleration and acceleration rate due to low-level turbulence, crew compartment.

EYD. The frequency response characteristics of the SAS were selected to provide control of the lower-frequency structural vibration modes. An indication of the effects of the prototype SAS on the stability of the low-frequency modes is given in Tables 2 and 3 for a low-level condition (350,000 lb and 350 KEAS). Table 2 presents the frequency and damping values for the low-frequency lateral-directional degrees of freedom for both the airplane with EYD and the airplane with the yaw SAS. Table 3 presents the same information for the low-frequency longitudinal degrees of freedom for the basic airplane and the airplane with the pitch SAS. The mode description for the elastic degrees of freedom indicates the motion of the primary structural component in the damped vibration mode.

Crew-Compartment Accelerations

The expected improvement in turbulence induced acceleration and acceleration rate in the crew compartment with the SAS is shown in Figs. 13 and 14. The ratio of the rms acceleration and acceleration rate for the airplane with the SAS to that of the baseline airplane is plotted vs gross weight for low-level operation. The vertical acceleration data are shown in Fig. 13 and the lateral data in Fig. 14.

Conclusions

The conclusions discussed in the following paragraphs summarize this preliminary analytical evaluation of structural performance of the B-52 with an improved SAS. These conclusions cover the areas of fatigue damage, maximum expected load, stability, and crew-compartment acceleration environment. The improvements are stated in terms of the expected performance of the airplane with the SAS relative to the baseline airplane. The baseline airplane is the present airplane with the EYD and no pitch SAS. The conclusions are based on the structural locations and results presented in the previous section.

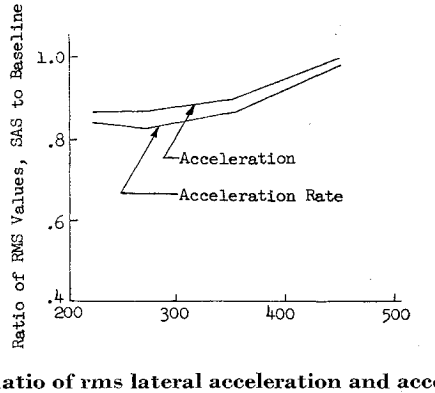

Fig. 14 Ratio of rms lateral acceleration and acceleration rate due to low-level turbulence, crew compartment.

Table 2 Effect of SAS on low-frequency lateral-directional modes, 350,000 lb gross weight, low level

Mode description	Damped frequency, cps		Damping ratio[a]	
	SAS	Baseline	SAS	Baseline
Spiral	0	0	115 sec[b]	143 sec[b]
Dutch roll	0.19	0.23	0.563	0.191
Body side bending	1.31	1.29	0.520	0.060
Wing vertical bending	1.38	1.39	0.070	0.067
Engine nacelle strut bending	1.98	1.97	0.020	0.021
Engine nacelle strut bending	2.03	2.03	0.006	0.006
Wing fore and aft bending	2.26	2.26	0.015	0.014
Wing torsion	2.74	2.74	0.030	0.032
Body torsion	3.10	3.01	0.186	0.092
Forward body side bending	3.46	3.45	0.012	0.012
Wing vertical bending	3.96	3.96	0.075	0.071

[a] Zero structural damping was assumed.
[b] Time to double amplitude.

Significant reductions are possible in aft fuselage fatigue-damage rates due to atmospheric turbulence. Reductions in aft fuselage damage rates of 80 to 90% are predicted with the SAS. Expected fatigue-damage rate reductions are about 90% for the vertical tail, 20 to 50% for the wing, and 40 to 80% for the horizontal tail.

The peak incremental stress on the vertical tail and aft fuselage, due to atmospheric turbulence, can be reduced by 35% with the SAS. Smaller but significant reductions in peak stress are also expected on the wing and horizontal tail. The vertical tail and aft fuselage are designed by gust criteria. The maximum expected gust loads on the wing and stabilizer are only about 80% of the critical design loads.

The stability of the B-52 is improved by the increased control authority and wider band frequency response of the SAS. The damping of the rigid airplane motions and the low-frequency aft fuselage vibration modes is increased by the SAS. Small reductions in rms vertical and lateral acceleration and acceleration rate are also predicted.

Table 3 Effect of SAS on low-frequency longitudinal modes, 350,000 lb gross weight, low level

Mode description	Damped frequency, cps		Damping ratio[a]	
	SAS	Baseline	SAS	Baseline
Short period pitch	0.42	0.43	0.621	0.412
Wing vertical bending	0.89	0.90	0.138	0.113
Wing fore and aft bending	1.78	1.86	0.040	0.040
Wing vertical bending	1.90	1.90	0.007	0.006
Engine nacelle strut bending	2.00	1.99	0.010	0.009
Engine nacelle strut bending	2.09	2.09	0.009	0.010
Body bending, wing torsion	2.44	2.39	0.082	0.059
Wing and body bending	3.08	3.07	0.009	0.008
Body bending, wing torsion	3.62	3.54	0.042	0.024

[a] Zero structural damping was assumed.

References

[1] Dempster, J. B. and Bell, C. A., "Summary of flight load environmental data taken on B-52 fleet aircraft," J. Aircraft 2, 398-406 (1965).

[2] Miner, M. A., "Linear cumulative damage method of analysis," J. Appl. Mech. 12 (September 1945).